eNeuro Accepted Manuscript

eNeuro

Research Article: New Research | Sensory and Motor Systems

Circuit and cellular mechanisms facilitate the transformation from dense to sparse coding in the insect olfactory system

https://doi.org/10.1523/ENEURO.0305-18.2020

Cite as: eNeuro 2020; 10.1523/ENEURO.0305-18.2020

Received: 4 August 2018
Revised: 31 October 2019
Accepted: 19 February 2020

This Early Release article has been peer-reviewed and accepted, but has not been through the composition and copyediting processes. The final version may differ slightly in style or formatting and will contain links to any extended data.

Alerts: Sign up at www.eneuro.org/alerts to receive customized email alerts when the fully formatted version of this article is published.

Copyright © 2020 Betkiewicz et al.
This is an open-access article distributed under the terms of the Creative Commons Attribution 4.0 International license, which permits unrestricted use, distribution and reproduction in any medium provided that the original work is properly attributed.

eNeuro Accepted Manuscript

1. Manuscript Title (50 word maximum)

Circuit and cellular mechanisms facilitate the transformation from dense to sparse coding in the insect olfactory system

2. Abbreviated Title (50 character maximum)

Modeling sparseness in the insect olfactory system

3. Author Names and Affiliations

Rinaldo Betkiewicz 1,2,3, Benjamin Lindner 1,3 & Martin P. Nawrot *1,2

1. Bernstein Center for Computational Neuroscience Berlin, Berlin, Germany

2. Computational Systems Neuroscience, Institute of Zoology, University of Cologne, Cologne, Germany

3. Department of Physics, Humboldt University Berlin, Berlin, Germany

* E-mail: martin.nawrot@uni-koeln.de

4. Author Contributions:

RB and MPN designed the research, RB implemented the model and analyzed the data, RB and MPN discussed results and analysis and drafted the manuscript; BL discussed results and analysis, and helped drafting the manuscript. All authors commented on the manuscript and gave final approval for publication.

5. Correspondence

martin.nawrot@uni-koeln.de

6. Number of Figures

(Seven) 7

7. Number of Tables

(One) 1

8. Number of Multimedia

eNeuro Accepted Manuscript

(Six) 6

9. Number of words for Abstract

220

10. Number of words for Significance Statement

120

11. Number of words for Introduction

453

12. Number of words for Discussion

1992

13. Acknowledgements

We thank Farzad Farkhooi for the initial network model and conceptual discussions.

14. Conflict of Interest

Authors report no conflict of interest

15. Funding

This research is supported by the German Research Foundation (grant no. 403329959) within the Research Unit 'Structure, Plasticity and Behavioral Function of the Drosophila mushroom body' (DFG-FOR 2705, https://www.uni-goettingen.de/en/601524.html). RB received a scholarship from the Research Training Group "Sensory Computation in Neural Systems" (DFG-RTG 1589) funded by the German Research Foundation.

eNeuro Accepted Manuscript

Circuit and cellular mechanisms facilitate the transformation from dense to sparse coding in the insect olfactory system

Rinaldo Betkiewicz[1,2,3], *Benjamin Lindner*[1,3], *Martin Paul Nawrot*[1,2]

[1] Bernstein Center for Computational Neuroscience Berlin, Berlin, Germany

[2] Computational Systems Neuroscience, Institute of Zoology, University of Cologne, Cologne, Germany

[3] Department of Physics, Humboldt University Berlin, Berlin, Germany

Short title: Modeling sparseness in the insect olfactory system

Keywords: sensory processing, odor trace, efficient coding, lateral inhibition, adaptation, spiking neural network

eNeuro Accepted Manuscript

Abstract

Transformations between sensory representations are shaped by neural mechanisms at the cellular and the circuit level. In the insect olfactory system encoding of odor information undergoes a transition from a dense spatio-temporal population code in the antennal lobe to a sparse code in the mushroom body. However, the exact mechanisms shaping odor representations and their role in sensory processing are incompletely identified. Here, we investigate the transformation from dense to sparse odor representations in a spiking model of the insect olfactory system, focusing on two ubiquitous neural mechanisms: spike-frequency adaptation at the cellular level and lateral inhibition at the circuit level. We find that cellular adaptation is essential for sparse representations in time (temporal sparseness), while lateral inhibition regulates sparseness in the neuronal space (population sparseness). The interplay of both mechanisms shapes spatio-temporal odor representations, which are optimized for discrimination of odors during stimulus onset and offset. Response pattern correlation across different stimuli showed a non-monotonic dependence on the strength of lateral inhibition with an optimum at intermediate levels, which is explained by two counteracting mechanisms. In addition, we find that odor identity is stored on a prolonged time scale in the adaptation levels but not in the spiking activity of the principal cells of the mushroom body, providing a testable hypothesis for the location of the so-called odor trace.

Significance Statement

In trace conditioning experiments, insects, like vertebrates, are able to form an associative memory between an olfactory stimulus and a temporally separated reward. Forming this association requires a prolonged odor trace. However, spiking responses in the mushroom body, the principal site of olfactory learning, are brief and bound to the odor onset (temporal sparseness). We implemented a spiking network model that relies on spike-frequency adaptation to reproduce temporally sparse responses. We found that odor identity is reliably encoded in the neurons' adaptation levels, which are mediated by spike-triggered calcium influx. Our results suggest that a prolonged odor trace is established in the calcium levels of the relevant neuronal population. This prediction has found recent experimental support in the fruit fly.

eNeuro Accepted Manuscript

Introduction

How nervous systems process sensory information is a key issue in systems neuroscience. Animals are required to rapidly identify behaviorally relevant stimulus features in a rich and dynamic sensory environment, and neural computation in sensory pathways is tailored to this need. Sparse stimulus encoding has been identified as an essential feature of sensory processing in higher brain areas in both, invertebrate (Perez-Orive et al., 2002; Szyszka et al., 2005; Ito et al., 2008; Turner et al., 2008; Honegger et al., 2011) and vertebrate (Hromádka et al., 2008; Vinje and Gallant, 2000; Wolfe et al., 2010; Isaacson, 2010) systems. Sparse representations provide an economical means of neural information coding (Laughlin and Sejnowski, 2003; Faisal et al., 2008) where information is represented by only a small fraction of all neurons (population sparseness) and each activated neuron generates only few action potentials (temporal sparseness) for a highly specific stimulus configuration (lifetime sparseness) (Kloppenburg and Nawrot, 2014).

The nervous systems of insects have limited neuronal resources and thus require particularly efficient coding strategies. The insect olfactory system is analogue to the vertebrate olfactory system and has become a popular model system for the emergence of a sparse code. We use a computational approach to study the transformation from a dense olfactory code in the sensory periphery to a sparse code in the mushroom body (MB), a central structure of the insect brain important for multimodal sensory integration and memory formation. A number of recent studies emphasized the role of sparse coding in the MB. In locusts, sparse responses were shown to convey temporal stimulus information (Gupta and Stopfer, 2012). In *Drosophila*, sparse coding was found to reduce overlap between odor representations and facilitate their discrimination (Lin et al., 2014). Consequently, sparse coding is an essential feature of plasticity models for olfactory learning in insects (Huerta and Nowotny, 2009; Wessnitzer et al., 2012; Ardin et al., 2016; Peng and Chittka, 2016; Müller et al., 2017) and theoretical work has emphasized the analogy of the transformation from a dense code in projection neurons (PNs) to a sparse code in Kenyon cells (KCs) with dimensionality expansion in machine learning methods (Huerta and Nowotny, 2009; Schmuker et al., 2014; Mosqueiro and Huerta, 2014).

Central to our modeling approach are two fundamental mechanisms of neural computation that are ubiquitous in the nervous systems of invertebrates and vertebrates. Spike-frequency adaptation (SFA) is a cellular mechanism that has been suggested to support efficient and sparse coding and to reduce variability of sensory representation (Benda and Herz, 2003;

eNeuro Accepted Manuscript

Farkhooi et al., 2011, 2013). Lateral inhibition is a basic circuit design principle that exists in different sensory systems, mediates contrast enhancement and facilitates stimulus discrimination (Kuffler, 1953; Hartline et al., 1956; Fuchs and Brown, 1984; Oswald et al., 2006). Both mechanisms are evident in the insect olfactory system. Responses of olfactory receptor neurons (ORNs), local interneurons (LNs) and PNs in the antennal lobe (AL) show stimulus adaptation (Nagel and Wilson, 2011; Bhandawat et al., 2007; Krofczik et al., 2009) and strong adaptation currents have been identified in KCs (Wüstenberg et al., 2004; Demmer and Kloppenburg, 2009). Lateral inhibition in the AL is mediated by inhibitory LNs (Wilson, 2013). It is crucial for establishing the population code at the level of PNs (Wilson et al., 2004; Olsen et al., 2010; Krofczik et al., 2009), for gain control (Stopfer et al., 2003; Olsen and Wilson, 2008), for decorrelation of odor representations (Wilson and Laurent, 2005), and for mixture interactions (Krofczik et al., 2009; Deisig et al., 2010; Capurro et al., 2012).

Taken together, we find that lateral inhibition and spike-frequency adaptation account for the transformation from a dense to sparse coding, decorrelate odor representations, and facilitate precise temporal responses on short and long time scales.

Methods

Spiking network model

A spiking network model with 3 layers (ORN, AL and MB, cf. Fig. 1A) was simulated using Brian 1.4 (Goodman and Brette, 2009). The model includes 35 ORN types, 284 ORNs per type, 35 PNs and LNs, and 1000 KCs. Each of the 35 LN-PN pairs constitute a glomerulus. Across insect species, the number of glomeruli varies from a few tens to several hundred, we based our model on the lower end of this range. The ratio between the number of PNs and KCs is roughly based on the data available in *Drosophila* (Turner et al., 2008).

The connections between the 3 network layers (ORNs, AL, MB) are feed-forward and excitatory. Within the AL, LNs provide lateral inhibition to PNs. ORNs provide input to PNs and LNs. All ORNs of the same receptor type target the same, single glomerulus. Every LN has inhibitory connections with all PNs, mediating unspecific lateral inhibition within the AL. Every KC receives 12 PN inputs on average (Szyszka et al., 2005; Turner et al., 2008). Connections between PNs and KCs were randomly drawn. Synaptic weights between all neurons are given in Table 1 for four different simulation conditions.

eNeuro Accepted Manuscript

	(i)	(ii)	(iii)	(iv)
w_{OL}	1 nS	1 nS	1 nS	1 nS
w_{OP}	1 nS	1.12 nS	1 nS	1.12 nS
w_{LP}	0 nS	3 nS	0 nS	3 nS
w_{PK}	5 nS	5 nS	5 nS	5 nS

Tab. 1 – Synaptic weights for w_{OL} (ORN-LN), w_{OP} (ORN-PN), w_{LP} (LN-PN) and w_{PK} (PN-KC) connections in different simulation conditions ((i)-(iv)).

Responses to a set of 7 stimuli, 50 trials each, and 3000 ms trial duration were simulated. Stimuli had a duration of 1000 ms and were presented at t=1000 ms. All neurons were initialized with membrane voltage set to the leak potential and the adaptation current set to zero. In order to achieve steady state conditions , simulations were pre-run for 2000 ms without recording the activity.

Receptor input

ORNs were modeled as Poisson spike generators, with evoked firing determined by a receptor response profile and a spontaneous baseline. In the absence of stimulus the spontaneous firing rate of all ORNs is set to $r_O^{BG} = 20$ Hz. In the presence of a stimulus the ORN firing rate is given by the summation of the spontaneous rate and an activation Δr_O:

$$r_O(t) = \begin{cases} r_O^{BG} + \Delta r_O & \text{for } t_{start} < t < t_{stop} \\ r_O^{BG} & \text{else} \end{cases}. \tag{1}$$

The intensity (amplitude) of ORN activation Δr_O is given by the receptor response profile that depends on receptor type and stimulus identity. Receptor activation follows a sine profile over half a period $(0 \dots \pi)$:

$$\Delta r_O = 40 \text{ Hz} \begin{cases} \sin(x\pi) & \text{for } 0 < x < 1 \\ 0 & \text{else} \end{cases},$$

$$x = \frac{(k_{RT} - k_S) \bmod N_{RT}}{N_A + 1},$$

where k_S is the stimulus index, k_{RT} the receptor type index, $N_{RT} = 35$ is the total number of receptor types and $N_a = 11$ is the number of receptor types activated by a stimulus. Given these parameters 35 different odor responses can be simulated ($k_S = 0 \dots 34$). This profile ensures that odor responses are evenly distributed across receptor types, while the

eNeuro Accepted Manuscript

choice of the sine shape was arbitrary. If the difference between the index of two stimuli Δk_s is small, those two stimuli are called similar, because they elicit largely overlapping responses. For $\Delta k_s > 12$ the responses do not overlap representing dissimilar stimuli.

Neuron model

PNs, LNs, and KCs were modeled as leaky integrate-and-fire neurons with conductance-based synapses and a spike-triggered adaptation (Treves, 1993) current I^A. We use the same set of cell parameters for all neuron types (cf. Table 2). This supports the generic character of our model and ensures that effects reported in this study are not a result of neuron-type specific parameters. The membrane potential of the i-th neuron from the PN, LN, and KC populations obeys:

$$c_m \frac{d}{dt} v_i^P = g_L \left(E_L - v_i^P\right) + g_i^{OP} \left(E_E - v_i^P\right) + g^{LP} \left(E_I - v_i^P\right) - I_i^A, \quad (2)$$

$$c_m \frac{d}{dt} v_i^L = g_L \left(E_L - v_i^L\right) + g_i^{OL} \left(E_E - v_i^L\right) - I_i^A, \quad (3)$$

$$c_m \frac{d}{dt} v_i^K = g_L \left(E_L - v_i^K\right) + g_i^{PK} \left(E_E - v_i^K\right) - I_i^A. \quad (4)$$

Membrane potentials follow a fire-and-reset rule. The fire-and-reset rule defines the spike trains of PNs, LNs and KCs denoted by $x_i^B = \sum_k \delta\left(t - t_{ik}^B\right)$ for the i-th neuron of type B. The spike trains of the ORN neurons are generated by a Poisson process with spike times t_{ijk}^O for the j-th receptor neuron of the k-th receptor type:

$$x_i^O(t) = \sum_j^{N_O/N_{glu}} \sum_k^{N_{glu}} \delta\left(t - t_{ijk}^O\right). \quad (5)$$

Synaptic conductances g_i obey:

$$\tau_E \frac{d}{dt} g_i^{OP} = -g_i^{OP} + \tau_E w_{OP} x_i^O(t), \quad (6)$$

$$\tau_E \frac{d}{dt} g_i^{OL} = -g_i^{OL} + \tau_E w_{OL} x_i^O(t), \quad (7)$$

$$\tau_I \frac{d}{dt} g^{LP} = -g^{LP} + \tau_I w_{LP} \sum_j^{N_{Glu}} x_j^L(t), \quad (8)$$

$$\tau_E \frac{d}{dt} g_i^{PK} = -g_i^{PK} + \tau_E \sum_j^{N_{Glu}} W_{ij} x_i^P(t). \quad (9)$$

eNeuro Accepted Manuscript

Adaptation currents I_i^A obey:

$$\tau_A \frac{d}{dt} I_i^A = -I_i^A + \tau_A \Delta I^A x_i(t) + \sqrt{2\tau_A \sigma_I^2}\,\xi(t)\,. \tag{10}$$

where τ_A is the time constant and ΔI^A the spike-triggered increase of the adaptation current. This phenomenological model of spike-triggered adaptation is biologically motivated by calcium-dependent outward potassium currents. Each action potential leads to an influx of a fixed amount of calcium and intracellular calcium is removed only slowly, resulting in an exponential decay of the intracellular calcium level. The last term reflects the diffusion approximation of channel noise (Schwalger et al., 2010), where $\xi(t)$ represents Gaussian, white noise. The variance of the adaptation currents I_i^A is given by σ_I^2.

Neuron Parameters		
membrane capacitance	c_m	289.5 pF
leak conductance	g_L	28.95 nS
leak potential	E_L	-70 mV
reset potential	V_R	-70 mV
threshold potential	V_T	-57 mV
refractory time	τ_{ref}	5 ms
Synaptic Parameters		
base synaptic weight	w_0	1 nS
PN-KC synaptic weight	w_{PK}	5 nS
excitatory synaptic potential	E_E	0 mV
excitatory time constant	τ_E	2 ms
inhibitory synaptic potential	E_I	-75 mV
inhibitory time constant	τ_I	10 ms
Adaptation Parameters		
spike triggered current	ΔI^A	0.132 nA
adaptation time constant	τ_A	389 ms
adaptation current variance	σ_I^2	87.1 pA^2

Tab. 2 – Parameters of the neuron model

Simulation conditions

Four different scenarios were simulated: without lateral inhibition and cellular adaptation (i), with lateral inhibition (ii), with cellular adaptation (iii) and with lateral inhibition and cellular adaptation (iv). We quantified the strength of lateral inhibition with a multiplicative factor α, that set by the synaptic weight w_{LP} in units of w_{OL}:

$$w_{LP} = \alpha w_0. \tag{11}$$

eNeuro Accepted Manuscript

Lateral inhibition is a network effect, conveyed by synaptic transmission, and was therefore compensated by scaling of synaptic weights. Weight scaling provides compensation during spontaneous as well as evoked activity. The scenario without lateral inhibition acts as a control condition, which deliberately does not include slow inhibitory synaptic dynamics.

In scenarios without cellular adaptation ((i), (ii)) the dynamic adaptation current was replaced by a compensatory static current $I_i^A \equiv I_0 = 0.38$ nA in the PN and LN populations, whereas in the KC population it was set to zero $I_i^A \equiv 0$ nA. In scenarios without lateral inhibition ((i),(iii)) the inhibitory weights w_{LP} were set to zero by setting $\alpha = 0$. The synaptic weight w_{OL} was adjusted to achieve a spontaneous LN firing rate of $\sim 8\,\mathrm{Hz}$ that is well within the experimentally observed range (Perez-Orive et al., 2002; Chou et al., 2010).

In all scenarios the spontaneous firing rate of PNs was set to ~ 8 Hz (Perez-Orive et al., 2002; Chou et al., 2010; Meyer et al., 2013), by adjusting the synaptic weights between the ORNs and the PNs w_{OP}.

Code Accessibility

Script files for model simulation are accessible at:
https://github.com/nawrotlab/SparseCodingInSpikingInsectModel.
Running the simulation requires Python 2.7, Brian 1.4 and numpy 1.11. All code was run on a x86-64 Linux machine.

`run_IF.py, run_saIF.py` - simulation scripts. Used to run the model in the absence and presence of spike-frequency adaptation, respectively. All paramaters are contained within the respective scripts. Runing the script file will save simulation results to file in the python pickle format.

`sim_code.py` - code of the neuron, input and network models.

Data analysis

Population firing rate

The spike count of the i-th neuron, in the k-th time bin with size Δt is given by:

$$n_{i,k} = \int_{(k-1)\Delta t}^{k\Delta t} dt\, x_i(t)\,. \tag{12}$$

eNeuro Accepted Manuscript

Population firing rates were obtained from the spike count in a small time bin ($\Delta t = 10$ ms)

$$\rho_k = \frac{1}{\Delta t} \langle n_{i,k} \rangle_i ,$$

where $\langle . \rangle_i$ indicates the population average. In addition population firing rates were averaged over 50 trials.

Sparseness measure

Sparseness of evoked KC responses was quantified by the widely used modified Treves–Rolls measure (Treves and Rolls, 1991; Willmore and Tolhurst, 2001):

$$s = 1 - \frac{\left(\frac{1}{N} \sum_{i=1}^{N} a_i \right)^2}{\frac{1}{N} \sum_{i=1}^{N} a_i^2},$$

where a_i indicates either the distribution of KC spike counts (population sparseness, for i between 1 and 1000), or binned KC population firing rate (temporal sparseness, $\Delta t = 50\, ms$, for i between 1 and 20). The sparseness measure takes values between zero and one, high values indicate sparse responses. Both measures were averaged over 50 trials.

Pattern overlap

We define the activation pattern for a given odor by a vector containing the evoked spike count for every neuron in a population. Pattern overlap between two similar odors A and B was calculated using an expression formally equivalent to Pearson's correlation coefficient:

$$\varrho_{AB,k} = \frac{N_{pop} \sum_i n_{ik} m_{ik} - \sum_i n_{ik} \sum_j m_{ik}}{\sqrt{N_{pop} \sum_i n_{ik}^2 - \left(\sum_i n_{ik} \right)^2} \sqrt{N_{pop} \sum_i m_{ik}^2 - \left(\sum_i m_{ik} \right)^2}}, \tag{13}$$

where n_{ik} and m_{ik} are the spike counts of the i-th neuron, k-th trial, in response to odor A and odor B ($\Delta k_S = 2$) respectively, and N_{pop} is the number of neurons in the population. The correlation coefficient was calculated both for the PN and the KC population, and averaged over 50 trials and 5 network realizations with randomly drawn PN-KC connectivity.

In addition, we consider trial-averaged activation patterns $\hat{n}_i = \frac{1}{N_{trial}} \sum_k n_{ik}$ and $\hat{m}_i = \frac{1}{N_{trial}} \sum_k m_{ik}$. Based on these trial-averaged patterns, the overlap between those patterns is given by:

$$\tilde{\varrho}_{AB} = \frac{N_{pop} \sum_i \hat{n}_i \hat{m}_i - \sum_i \hat{n}_i \sum_j \hat{n}_j}{\sqrt{N_{pop} \sum_i \hat{n}_i^2 - \left(\sum_i \hat{n}_i \right)^2} \sqrt{N_{pop} \sum_i \hat{m}_i^2 - \left(\sum_i \hat{m}_i \right)^2}}. \tag{14}$$

eNeuro Accepted Manuscript

The overlap between the trial-averaged patterns was calculated both for the PN and the KC population, and averaged over 5 network realizations with randomly drawn PN-KC connectivity.

Lateral inhibition scaling with parameter α In order to test if the decrease of overlap was robust for different strengths of lateral inhibition, the synaptic weight w_{OP} was adjusted as follows:

$$w_{OP} = w_0 \left(1 + \alpha b\right), \tag{15}$$

where b was estimated from simulations under the condition that for a range of lateral inhibition strengths ($\alpha \in [0, 9]$) the spontaneous PN firing rate was close to 8 Hz.

Decoding analysis

Odor identity was recovered from odor representations by Gaussian naive Bayes classification (Rish, 2001), using the scikit-learn package (Pedregosa et al., 2012). Training and testing data consisted of simulated odor representations for a set of seven stimuli ($k_S = 0, 2, \ldots, 12$), 50 trials each. Classification was repeated for every time bin ($\Delta t = 50$ ms, 60 bins total) for PN spike counts, KC spike counts, or amplitudes of KC adaptations currents. Data was divided into a training and testing set using a 3-fold cross-validation procedure. Decoding accuracy was estimated by the *maximum a posteriori* method and is given by the fraction of successful classification trials divided by the total number of test trials.

Results

Spiking network model of the olfactory pathway with lateral inhibition and spike-frequency adaptation

We designed a spiking network model that reduces the complexity of the insect olfactory processing pathway to a simplified three-layer network (Fig. 1A) that expresses the structural commonality across different insect species: an input layer of olfactory receptor neurons (ORNs), subdivided into different receptor types, the AL, a first order olfactory processing center, and the MB. Furthermore, the model combines two essential computational elements: (i) lateral inhibition in the AL, and (ii) spike-frequency adaptation in the AL and the MB.

eNeuro Accepted Manuscript

The processing between the layers is based on excitatory feedforward connections. Converging receptor input from all ORNs of one type is received by spatially confined subunits of the AL called glomeruli. In our model, glomeruli are represented by a single uniglomerular PN and a single inhibitory local interneuron (LN). In the MB, each KC receives on average 12 PN inputs (Szyszka et al., 2005), based on a random connectivity between the AL and the MB (Caron et al., 2013). All neurons in the AL and the MB were modeled as leaky integrate-and-fire neurons with spike-triggered adaptation. Based on evidence from theoretical (Schwalger et al., 2010) and experimental studies (Fisch et al., 2012), adaptation channels cause slow fluctuations. We accounted for this fact by simulating channel noise in the slow adaptation currents (cf. Methods).

We simulated ORN responses to different odor stimuli. Single ORN responses were modeled in the form of Poisson spike trains with firing rates dependent on the receptor type and stimulus identity. The relationship is set by a receptor response profile (Fig. 1B left) which determines ORN firing rates of all receptor types for a given stimulus. Responses to different stimuli are generated by shifting the response profile along the receptor space. The offset between any two stimuli reflects their dissimilarity - similar stimuli activate overlapping sets of olfactory receptors, whereas dissimilar stimuli activate largely disjoint sets of receptors. Stimuli were presented for one second, reflected by a step-like increase of ORN firing rate.

In the absence of stimuli, ORNs fired with a rate of 20 Hz reflecting their spontaneous activation (Nagel and Wilson, 2011). Both LNs and PNs receive direct ORN input. We tuned synaptic weights of the model to match physiologically observed firing rates of PNs and LNs, which are both about 8 Hz (Perez-Orive et al., 2002; Chou et al., 2010; Meyer et al., 2013) (for details see Methods). Lateral inhibition and spike-frequency adaptation, the neural mechanisms under investigation, both provide an inhibitory contribution to a neuron's total input. In our model, spike-frequency adaptation is a cellular mechanism mediated by a slow, spike-triggered, hyperpolarizing current in LNs, PNs and KCs, whereas a global lateral inhibition in the AL is mediated by LNs with fast synapses that receive input from a single ORN type and inhibit all PNs in a uniform fashion.

Odor responses at the AL and the MB level of the spiking network model

Figure 1B illustrates PN and KC responses to one odor. PNs driven by the stimulus showed a strong transient response at the stimulus onset, a pronounced adaptation during the stimu-

eNeuro Accepted Manuscript

Fig. 1 – Olfactory network model structure and odor response. *(A)* Network structure resembles the insect olfactory pathway with three main processing stages. In each glomerulus (dashed circles), a PN (blue) and a LN receive convergent ORN input (red) by one receptor type (RT). Each LN provides unspecific lateral inhibition to all PNs. KCs (orange) receive on average 12 inputs from randomly chosen PNs. *(B)* Receptor response profile (red bars; AL input) depicts the evoked firing rate for each ORN type. Evoked PN spike counts (dashed blue line; AL output) follow the ORN activation pattern. Raster plots depict single trial responses of PNs (blue) and KCs (orange). Presentation of an odor during 1000 ms is indicated by the shaded area. Population firing rates were obtained by averaging over 50 trials. PN spikes display a temporal structure that includes evoked transient responses at stimulus on- and offset, and a pronounced inhibitory post-odor response. PN population rate was averaged over PNs showing "on" responses (blue) and "off" responses (cyan). KC spikes were temporally sparse with majority of the spikes occurring at the stimulus onset. Supporting Fig. 1-1 and Fig. 1-2 (available online) show odor responses with adaptation disabled in the KC and PN population, respectively.

lus, and a period of silence after stimulus offset due to the slow decay of the strong adaptation current. This resembles the typical phasic-tonic response patterns of PNs (Bhandawat et al., 2007; Nawrot, 2012; Meyer et al., 2013).

PNs receiving direct input from ORNs activated by the stimulus, showed a strong response at the stimulus onset. Interestingly, the population firing rate over these PNs revealed that the "on" response follows a biphasic profile with an early and a late component. In addition, PNs with no direct input from stimulated ORNs showed an "off" response at the stimulus offset. Non-driven PNs were suppressed during a short period after stimulus onset, and showed reduced firing during the tonic response. The PN population response consisted of complex activations of individual PNs with phases of excitation and inhibition. Hence, in the AL, odors were represented as spatio-temporal spike patterns across the PN population.

At the level of the MB, KCs typically show none or very little spiking during spontaneous activity and respond to odors with only a few spikes in a temporally sparse manner (Perez-Orive et al., 2002; Ito et al., 2008; Turner et al., 2008). In our model, synaptic weights between PNs and KCs were tuned to match the very low probability of spontaneous firing. Resulting KC responses were temporally sparse. Due to the negative feedback mediated by strong spike-frequency adaptation, most KC spikes were confined to stimulus onset. Notably, we also found that KCs sometimes exhibited "off" responses. These KC "off" spikes occurred very rarely, because they are driven by the PN "off" response, which is much weaker compared to the PN "on" response. Timing and amplitude of temporally sparse responses are in good quantitative agreement with in vivo KC recordings (Ito et al., 2008).

Dense and dynamic odor representations in the AL

In order to explore effects of lateral inhibition and cellular adaptation on stimulus representations, we simulated odor responses in conditions in which we separately deactivated one

eNeuro Accepted Manuscript

or both mechanisms. Lateral inhibition was deactivated by setting the inhibitory synaptic weight between LNs and PNs to zero and simultaneously reducing the value of the excitatory synaptic weight between ORNs and PNs, such that the spontaneous firing rate of 8 Hz was kept. Adaptation was deactivated by replacing the dynamic adaptation current by a constant current with an amplitude that maintained the average spontaneous firing rate.

Figure 2 illustrates the separate effects of lateral inhibition and adaptation on odor responses in the PN population. In all conditions, PNs fired spontaneously before stimulation due to spontaneous ORN activation. PNs driven by stimulation receive input from ORNs that were activated by the presented odor. In the absence of adaptation and lateral inhibition (Fig. 2 (i)) the stimulus response followed the step-like stimulation and showed no further temporal structure. In the presence of lateral inhibition (Fig. 2 (ii)), PNs not driven by the stimulus were strongly suppressed. Adaptation alone (Fig. 2 (iii)) resulted in a phasic-tonic response profile with a high phasic peak amplitude immediately after stimulus onset. In the presence of both mechanisms (Fig. 2 (iv)) we observed the characteristic phasic-tonic PN response. The transient response was reduced in peak amplitude, and, interestingly, followed a biphasic profile with an early and a late component.

Fig. 2 – Lateral inhibition and cellular adaptation shape PN odor response dynamics. *(A)* Single trial PN spiking responses simulated with (right column) and without (left column) lateral inhibition, and with (bottom row) and without (top row) adaptation. Presentation of a single odor during 1000 ms is indicated by the shaded area. With adaptation PNs display a temporal structure that includes a transient and a tonic response, and a pronounced inhibitory post-odor response. *(B)* Trial averaged population firing rate: PNs driven by stimulation (blue) and remaining PNs (cyan). Panels (i)-(iv) indicate presence and absence of lateral inhibition and adaptation as in (A). In the presence of lateral inhibition firing rates during stimulation are reduced. In the presence of lateral inhibition and adaptation (iv) PNs show either transient "on" responses (blue) or "off" responses (cyan). Panels A (iv) and B (iv) are reproduced in Fig. 1B. Supporting Fig. 2-1 (available online) shows PN tuning profiles and input-output relation.

In our model, the interaction of lateral inhibition and the intrinsic adaptation currents in LNs and PNs accounts for biphasic PN responses. Because LNs are adapting, lateral inhibition is strongest at stimulus onset. Most PNs were initially suppressed and showed a slightly delayed response, whereas the initial response of PNs with strong input (early component) was not affected. Fast and delayed PN responses have also been found experimentally in the honeybee (Strube-Bloss et al., 2012). Model evidence for the interplay of cellular and network mechanisms behind biphasic PN responses was found in the pheromone system of the moth (Belmabrouk et al., 2011).

eNeuro Accepted Manuscript

Spike-frequency adaptation supports temporal sparseness in the MB

To isolate the contributions of adaptation and lateral inhibition (the latter present only at the AL level) to odor responses at the MB level, we again tested the four conditions by deactivating one or both mechanisms. In all four conditions, KCs were almost silent and spiked only sporadically during spontaneous activity, whereas amplitude and temporal profile of their odor response differed across conditions (Fig. 3).

In the presence of adaptation we observed temporally sparse responses (Fig. 3 (iii)-(iv)). KCs typically responded with only 1-3 spikes (mean spikes per responding KC were slightly above one, compare $\overline{x}$ in Fig. 3B (iii),(iv)). Due to the negative feedback mediated by strong spike-frequency adaptation, most KC spikes were confined to stimulus onset.

In the absence of adaptation and regardless of the presence (Fig. 3 (i)) or absence (Fig. 3 (ii)) of lateral inhibition, responding KCs fired throughout stimulation, because they received persistently strong input from PNs. Such persistent KC responses are in disagreement with experimental observations (Perez-Orive et al., 2002; Ito et al., 2008; Turner et al., 2008).

Fig. 3 – Odor response dynamics of the KC population. Figure layout as in Fig. 2. *(A)* Single trial population spike raster responses. *(B)* Trial averaged KC population firing rate. Numbers to the right indicate the fraction of activated KCs (n_a) and the mean number of spikes per activated KC during stimulation ($\bar{x}$). Without adaptation (i,ii) KCs spike throughout stimulation because PN drive is strong and persistent. The fraction of activated KCs drops in the presence of lateral inhibition (ii,iv). With adaptation (iii,iv) most of KC spikes are confined to the stimulus onset, indicating temporally sparse responses. We note that spontaneous KC activity is extremely low (0.03 Hz) in accordance with experimental results (Ito et al., 2008). Panels A (iv) and B (iv) are reproduced in Fig. 1B.

We quantified temporal sparseness of KC responses by calculating a measure modified from (Treves and Rolls 1991, cf. Methods). Comparison of temporal sparseness across the four conditions confirms that KC responses were temporally sparse only in the presence of adaptation whereas lateral inhibition had no effect on temporal sparseness (Fig. 4A). Selective absence of adaptation in the KC population (supporting Fig. 1-1) did not have an effect on KC temporal sparseness (supporting Fig. 4-1A). This is due to high KC spiking threshold that requires strong input and ensures sparse responses. Selective absence of adaptation in the PN population (supporting Fig. 1-2) led to persistent tonic KC responses, in addition to the onset KC responses. This is due to strong tonic PN input leading to reduced KC temporal sparseness.

eNeuro Accepted Manuscript

Fig. 4 – Quantification of temporal and population sparseness in the KC population. Sparseness was measured in the absence ($\alpha = 0$) and presence ($\alpha = 3$) of lateral inhibition, and the presence (black bars) and absence (gray bars) of spike-frequency adaptation. The sparseness measure was averaged over 50 trials. Error bars indicate standard deviation. A value of one corresponds to maximally sparse responses. *(A)* Adaptation promotes temporal sparseness. *(B)* Lateral inhibition in the AL promotes KC population sparseness. Supporting Fig. 4-1 (available online) shows temporal sparseness when spike-frequency adaptation was disabled in the PN or KC population, and population sparseness for different numbers of PN inputs per KC.

Lateral inhibition supports population sparseness in the MB

We observed that the fraction of responding KCs was considerably lower in the presence of lateral inhibition (compare n_a across panels in Fig. 3B). We recall that lateral inhibition in our model is acting on PNs. The transient PN population rate response showed a biphasic peak in the presence of lateral inhibition. Effectively, the transient PN response was broadened in time and its amplitude was reduced (compare Fig. 2B (iii),(iv)). As a result, KCs received lower peak input from PNs. How does this affect KC responses on a population level?

We visualized MB odor representations with activation patterns obtained by arranging KC spike counts evoked by two similar odors on a 30x30 grid in arbitrary order (Fig. 5A). In the absence of lateral inhibition (Fig. 5A top), a majority of the KC population was activated by both tested odors Each of the 1000 KCs receives input from, on average, 12 PNs and thus from about one third of the total PN population. KCs are readily activated by the strong PN input within a short time window following stimulus onset. Matching experimental results, KCs responded with 1-3 spikes. Turner et al. (2008) counted 2.2 - 4.9 KC response spikes in *Drosophila* in-vivo intracellular recordings. Using extracellular single unit recordings, (Ito et al., 2008) reported that moth KCs typically respond with a single spike and a maximum of 5 spikes. These numbers correspond to the apparent KC responses in the locust displayed in Broome et al. (2006).

In the presence of lateral inhibition (Fig. 5A bottom), the fraction of activated KCs was reduced substantially (KCs activated, trial averaged: 9%, std: 3%). Again, this matches well the experimentally reported fraction of stimulus activated KCs in the range of 5-10% as measured in *Drosophila* (Turner et al., 2008; Honegger et al., 2011) and 6-11% in the locust (Perez-Orive et al., 2002; Broome et al., 2006). In our model, due to the lower peak input from PNs, only KCs with large numbers of PN inputs are likely to be activated. Therefore the KC population responds more selectively. The range of individual KC responses (1-3 spikes) was not affected. These activation patterns demonstrate that the MB odor representations

eNeuro Accepted Manuscript

are sparse on a population level, as each odor is represented by the activity of a small fraction of the KC population.

Fig. 5 – Lateral inhibition in the AL facilitates population sparseness and reduces pattern correlation in the MB. Spike counts (single trial) of 900 randomly selected KCs in response to two similar odors ("Odor A" and "Odor B") arranged on a 30x30 grid in the absence (top row) and in the presence (bottom row) of lateral inhibition. Inactive KCs are shown in black. *(A)* In the absence of lateral inhibition KCs readily responded to both odors, resulting in an activation pattern where most KCs are active. In the presence of lateral inhibition both odors evoked sparse KC activation patterns. *(B)* Superposition of responses to the two odors. KCs that were activated by both odors are indicated by hot colors (color bar denotes spike count of the stronger response). KCs that were activated exclusively by one of the two odors are indicated in gray. The fraction of KCs that show overlapping responses is reduced in the presence of lateral inhibition. (C) Pattern correlation between the single trial responses in (A) to the two odors obtained for PN (blue) and KC (orange) spikes counts, in the absence ($\alpha = 0$) and presence ($\alpha = 3$) of lateral inhibition. Dashed line indicates pattern correlation of the input (ORNs). Pattern correlation was retained at the AL and reduced at the MB level. Lateral inhibition in the AL reduced pattern correlation in KCs but not in PNs.

To quantify population sparseness of odor representations in the MB, we again calculated a sparseness measure (cf. Methods). Population sparseness increased in the presence of lateral inhibition, independent of spike-frequency adaptation (Fig. 4B). In the presence of lateral inhibition and spike-frequency adaptation, both population and temporal sparseness were in qualitative and quantitative agreement with experimental findings (Perez-Orive et al., 2002; Szyszka et al., 2005; Ito et al., 2008; Turner et al., 2008). We note that population sparseness also depends on the connectivity parameters of the model (see Discussion). In particular, increasing the average number of PN inputs per KC decreased population sparseness, whereas reducing this number resulted in an increase of population sparseness (cf. supporting Fig. 4-1). However, lateral inhibition has a dominant effect on population sparseness, irrespective of the PN-KC connectivity (cf. supporting Fig. 4-1). Taken together, odor representations at the MB level were characterized by a small fraction of the KC population responding with a small number of spikes.

Decorrelation of odor representations between AL and MB

In our model, lateral inhibition in the AL increased population sparseness of MB odor representations. Does an increased KC population sparseness lead to less overlap between MB odor representations? We visualized the overlap between odor representations in the MB by overlaying KC activation patterns in response to two similar odors (Fig. 5B). KCs responding exclusively to odor A or odor B are shown in gray, whereas KCs responding to both odors are color coded. With lateral inhibition (Fig. 5B bottom), most of the KC responses were unique to odor A or odor B and only few KCs were activated by both odors. In contrast, with lateral inhibition deactivated (Fig. 5B top), the ratio of KCs with

eNeuro Accepted Manuscript

unique responses to the total number of activated cells was low, indicating highly overlapping responses. We quantified the overlap between odor representations evoked by two similar odors in the PN and the KC population. To this end, we calculated an overlap measure (formally equivalent to Pearson's correlation coefficient, cf. Methods) between spike count patterns evoked by odors A and B (Fig. 5C). Interestingly, PNs retained the overlap of the input, independent of lateral inhibition. In contrast, KC representations showed a reduced overlap that decreased even further in the presence of lateral inhibition.

We tested how scaling of the lateral inhibition strength affected the pattern overlap in PN and KC odor representations. To this end, we varied the strength of lateral inhibition (α) in the AL by increasing the strength of inhibitory synapses and adjusting feedforward weights (see Methods). In addition, we calculated pattern correlations in the absence of adaptation. As before, pattern correlation was calculated for two similar odors that activated an overlapping set of receptors. In the absence of adaptation, lateral inhibition decorrelated odor representations in both populations (Fig. 6B). However, for increasing strength of lateral inhibition this leads to an unphysiological regime with unrealistic low fraction of KCs that show a response (supporting Fig. 6-1B). In the presence of adaptation, increasing lateral inhibition had different effects on the PN and KC population (Fig. 6A). In PNs the correlation of the input was retained for all tested values of lateral inhibition. In KCs pattern correlation first decreased for weak to moderate lateral inhibition strength but then increased for strong lateral inhibition. For an intermediate strength of the inhibitory weights the pattern correlation between KC responses to similar odors attained a minimal value. For comparison, the bottom panels of Fig. 6 show the overlap $\tilde{\varrho}$ between the trial-averaged activation patterns, both in the presence (Fig. 6C) and absence (Fig. 6D) of adaptation. For PN representations both measures (ϱ and $\tilde{\varrho}$), indicate the same overlap (compare blue lines in (Fig. 6AB and 6CD). For KC representations, the measure based on averaged spike counts ($\tilde{\varrho}$) is generally higher, whereas the minimum for intermediate strength of lateral inhibition is shallower (orange line in 6C). Overlap based on spike count patterns recorded in single trials decreases when responses are subject to trial-to-trial variability. In contrast, by averaging the patterns first, the effect of trial-to-trial variability is reduced. The comparison of both overlap measures indicates that in our model KC representations are more variable across trials compared with PN representations.

What is the explanation for the observed minimum in pattern overlap? The minimum of pattern overlap for $\alpha = 3$ coincides with the minimum of the fraction of activated KCs

eNeuro Accepted Manuscript

(supporting Fig. 6-1). A lower fraction of responding KCs can be understood as increased selectivity of KC responses. Both can be linked to changes of the PN input with two counteracting effects. For low strengths of lateral inhibition the amplitude of transient PN input decreases with lateral inhibition due to temporal dispersion of response spikes across the PN population (cf. Fig. 2B (iv)). KC selectivity increases, whereas pattern overlap decreases.

The increase of pattern overlap for $\alpha \geq 4$ is caused by common noise in KCs. The reason for the common noise are cross-correlations of PN output spike-trains. Their mean pairwise cross-correlation is zero in the absence of inhibition, and increases with α (cf. supporting Fig. 6-2). Due to increased cross-correlation of their inputs, KCs are more easily activated. However for $\alpha \geq 4$, KC responses are increasingly stimulus unspecific due to common noise and overlapping inputs. Taken together, for weak to intermediate lateral inhibition KC selectivity increases, responses remain stimulus specific and become more sparse. For strong lateral inhibition ($\alpha \geq 4$), the fraction of activated KCs increases as KC responses become more unspecific, driven by common noise.

In general, a reduction of pattern correlation from PN to KC representations is characteristic for the insect MB (Laurent, 2002). Furthermore low overlap between KC representations has been found to facilitate discrimination of odors (Campbell et al., 2013). We therefore choose the intermediate strength of the inhibitory weights ($\alpha = 3$) as a reference point in our model.

Fig. 6 – Pattern correlation in the antennal lobe and the mushroom body depend on lateral inhibition strength α. The correlation coefficient ρ_{AB} between the response patterns to two similar odors was calculated and averaged over 50 trials and 5 network realizations for PNs *(blue)* and KCs *(orange)*. Error bars indicate standard deviation over trials and network realizations. Pattern correlation of the input is indicated by the dashed line. Input correlation is high because similar odors activate largely overlapping set of receptors. *(A)* In the presence of adaptation, pattern correlation in PNs (*blue*) stays close to the input correlation for all values of lateral inhibition strength. In KCs (*orange*) the correlation decreases for small values of lateral inhibition strength, and increases for large values of lateral inhibition strength. Pattern correlation in KCs is minimal for $\alpha = 3$. *(B)* In the absence of adaptation, pattern correlation decreases with the lateral inhibition strength both in PNs and KCs. The decrease is stronger in KCs. *(CD)* Pattern correlation $\tilde{\varrho}_{AB}$ was calculated based on evoked, trial-averaged spike counts in the presence (C) and absence (D) of lateral inhibition. The correlation coefficient between the trial-averaged response patterns to two similar odors was calculated and averaged over 5 network realizations. Error bars indicate standard deviation over network realizations. In the presence of adaptation (C) the overlap between trial-averaged KC representations of two similar odors (orange) shows a minimum for intermediate strengths of lateral inhibition ($1 \leq \alpha \leq 3$). At the minimum, the KC overlap is below the overlap between trial-averaged PN representations. In the absence of adaptation the overlap between trial-averaged KC representations is generally lower than the overlap between trial-averaged PN representations for all strengths of lateral inhibition. Supporting Fig. 6-1 and Fig. 6-2 (available online) show the mean fraction of activated KCs and mean pairwise KC cross-correlation, respectively.

eNeuro Accepted Manuscript

Odor encoding on short and long time scales

Next, we tested if in our model the information about stimulus identity is contained in AL and MB odor representations by performing a decoding analysis in subsequent time bins of 50 ms (cf. Methods). In PNs decoding accuracy peaked during stimulus on- and offset (Fig. 7A). Both peaks coincide with a state of transient network activity caused by the odor on- or offset. The "on" and the "off" responsive PNs establish odor representations optimized for discrimination. After stimulus onset, decoding accuracy dropped but remained on a plateau well above chance level. Remarkably, after stimulus offset, odor identity could be decoded for an extended time period (several hundreds of ms) albeit with a reduced accuracy. Such odor after effects have been demonstrated previously in experiments (Szyszka et al. (2011), cf. Discussion).

In KCs decoding accuracy was above chance level only in the first 2-3 time bins (about 100 ms) after stimulus onset (Fig. 7B). In all other time bins decoding accuracy remained at chance level. Because the spiking activity in the KC population is temporally sparse, the continuous information at the AL output is lost in the MB spike count representation. This raises the question whether and if so how the information could be preserved in the MB throughout the stimulus. The intrinsic time scale of the adaptation currents might potentially support prolonged odor representations (Fig. 7C). We therefore repeated the decoding analysis on the adaptation currents measured in KCs (Fig. 7D). Indeed, the stimulus identity could reliably be decoded based on the intensity of the adaptation currents in subsequent time bins of 50 ms. Decoding accuracy peaked after stimulus onset and then slowly decreased. Remarkably, the time scale of the decay is comparable during and after stimulation. Because KCs show very little spontaneous activity, the decoding accuracy after stimulation decays with the adaptation time constant. This is due to the exponential decay of the adaptation currents evoked by stimulation, and the stochastic adaptation current fluctuations in the background due to channel noise.

Fig. 7 – Decoding of odor identity indicates a prolonged and reliable odor information in KC adaptation currents. *(A,B,D)* Decoding accuracy was calculated for non-overlapping 50 ms time bins, based on a set of seven stimuli (chance level ≈ 0.14) presented for one second (shaded area). Blue shading indicates standard deviation obtained from a cross-validation procedure (see Methods). *(A)* Decoding of odor identity from PN spike counts. Decoding accuracy peaks at odor on- and offset, and remains high after stimulation. *(B)* Decoding of odor identity from KC spike counts. Decoding accuracy is above chance only in the first three bins following stimulus onset. *(C)* Adaptation current amplitudes (single trial, hot colors in arbitrary units) of 100 selected KCs in response to "odor A" (top) and "odor B" (bottom). *(D)* Decoding of odor identity from KC adaptation currents. Decoding accuracy peaks 150 ms after odor onset, then drops during stimulation but remains high and is sustained after odor offset.

eNeuro Accepted Manuscript

Discussion

We investigated the transformation between dense AL and sparse MB odor representations in a spiking network model of the insect olfactory system. Our generic model demonstrates lateral inhibition and spike-frequency adaptation as sufficient mechanisms underlying dynamic and combinatorial responses in the AL that are transformed into sparse MB representations. To simulate responses to different odors we incorporated simple ORN tuning and glomerular structure in our model. This approach allows us to investigate how different odors are represented in the AL and MB population activity and asses information about odor identity contained in respective odor representations. We inspected overlap between odor representations in both populations. Sparse coding reduces overlap between representation, as has been predicted on theoretical grounds (Marr, 1969; Albus, 1971; Kanerva, 1988) and shown for MB odor representations (Szyszka et al., 2005; Turner et al., 2008; Lin et al., 2014). Similarly, our model shows pattern decorrelation in the MB but not in the AL.

Post-odor responses

In our model, we found "on" and "off" responsive PNs. At the stimulus offset, the "off" responsive PNs transiently increase, whereas the "on" responsive PNs transiently decrease their firing rate (cf. Fig. 2). "On" responsive PNs remain adapted beyond stimulus offset. Their excitability thus stays reduced until the slow adaptation current has decayed. In contrast, in "off" responsive PNs increased lateral inhibition during stimulation causes a below-baseline adaptation level throughout the stimulus and thus an increased excitability. In effect, the odor-evoked and the post-odor PN activation patterns are reversed, i.e. anti-correlated (not shown). This result matches well the experimental observations in honeybee (Szyszka et al., 2011; Nawrot, 2012; Stierle et al., 2013) and *Drosophila* (Galili et al., 2011) PNs. Those results show highly correlated response patterns throughout stimulation, and stable but anti-correlated post-odor response patterns.

Differential mechanism underlying temporal and population sparseness in KCs

In our model, the two mechanisms underlying temporal sparseness and population sparseness act independently.

eNeuro Accepted Manuscript

Temporal sparseness of KC responses in our model compares well to the experimentally recorded spiking responses in *Drosophila*, locust and moth (Perez-Orive et al., 2002; Ito et al., 2008; Turner et al., 2008), and to calcium imaging experiments in the honeybee (Szyszka et al., 2005). The model proposed here solely relies on spike-frequency adaptation for temporally sparse responses. On a cellular level, strong adaptation currents in KCs, which are suitable for generation of sparse responses, have been found in the honeybee (Wüstenberg et al., 2004) and cockroach (Demmer and Kloppenburg, 2009). In the model temporal sparseness is not affected by the deactivation of lateral inhibition, a finding supported by a previous study by Farkhooi et al. (2013).

Several studies have suggested that either feedforward inhibition (Assisi et al., 2007) or feedback inhibition (Szyszka et al., 2005; Papadopoulou et al., 2011; Gupta and Stopfer, 2012; Lei et al., 2013; Kee et al., 2015) causes temporally sparse responses. The existence of inhibitory feedback neurons in the MB has been demonstrated experimentally in different insect species (cockroach: Takahashi et al. (2017), *Drosophila:* Liu and Davis (2009), honeybee: Grünewald (1999), locust: Papadopoulou et al. (2011)), whereas evidence for feedforward inhibition to the MB is lacking (Gupta and Stopfer, 2012). Our model demonstrates that temporally sparse responses can be obtained without an inhibitory circuit motive. There is further evidence for a GABA-independent mechanism for the temporal shortening of KC responses. Calcium imaging studies in *Drosophila* (Lei et al., 2013; Lin et al., 2014) and in the honeybee (Farkhooi et al., 2013; Froese et al., 2014) showed that the temporal profile of KCs' fast response dynamics is preserved even if GABAergic inhibition is blocked.

What could be the benefit of temporally sparse responses in KCs? We hypothesize that temporal sparseness is an important strategy for the system to follow fast transient inputs rather than representing static input. The typical lab experiment uses controlled odor stimuli that are presented with static intensity for up to several seconds. However, in a natural setting, olfactory inputs are highly dynamic (Vickers et al., 2001). Natural odor plumes do not represent a gradient intensity due to diffusion. Rather, odors distribute in space and time in a filamentous structure (Celani et al., 2014; Vickers, 2000) and filaments from different odors do not mix perfectly (Szyszka et al., 2012). Due to wind and animal movement - particularly relevant for flying insects - the olfactory input will generally be highly dynamic in time resulting in fast and steep changes of odor concentration whenever the animal encounters an odor filament. In such an on-off scenario, temporally sparse responses in KCs might enable processing of rapid odor filament encounters. We hypothesize that the KC population

eNeuro Accepted Manuscript

provides a temporally sparse representation of each filament's odor identity with a single or few spikes in each KC. The system is thus able to track individual odor filament encounters over time and the animal can adapt its behavior accordingly, e.g. during odor source location in foraging flights (Budick, 2006; Van Breugel and Dickinson, 2014; Egea-Weiss et al., 2018). At the periphery it has been shown that the olfactory receptor neurons in various insect species are able to follow fast repeating olfactory input pulses even for high pulse frequencies (Vickers et al., 2001; Szyszka et al., 2014). Our results show that the mechanism of spike-frequency adaptation is able to generate temporally sparse responses to the onset of an odor and thus to detect temporal changes in the olfactory input rather than encoding the persistence of a stimulus. Adaptation has previously been implicated as a means to compute the temporal derivative of sensory input (Tripp & Eliasmith, 2010; Lundstrom et al., 2008; Farkhooi et al., 2013). A second advantageous property of spike frequency adaptation is that it facilitates the reliability of individual responses and significantly reduces the variability in the number of response spikes across repeated stimulus representation (Farkhooi et al., 2011; Farkhooi et al, 2013). Temporal sparseness is not limited to the insect MB and has been discovered in diverse sensory systems, notably in mammalian sensory cortices (e.g. Vinje and Gallant 2000; Hromádka et al. 2008; Wolfe et al. 2010; Isaacson 2010) where it has also been linked to the encoding of temporally dynamic input in natural scences (e.g. Yen et al. 2010; Haider et al. 2010). We suggest that spike-frequency adaptation is a general mechanisms across sensory systems and taxa supporting reliable temporally sparse responses under natural sensory input conditions.

The KC population sparseness in our model matches qualitatively and quantitatively with experimental estimates from electrophysiological responses in locust and *Drosophila* (Perez-Orive et al., 2002; Turner et al., 2008) and from calcium imaging in *Drosophila* (Honegger et al., 2011). Our model shows sparse KC responses on a population level in the presence but not in the absence of lateral inhibition. Calcium imaging experiments in the honeybee (Froese et al., 2014) have shown that inactivating GABA transmission disrupts population sparseness, in line with our modeling results. In *Drosophila,* feedback inhibition contributes to the population sparseness of KCs, as blocking of feedback inhibition reduced population sparseness and undermined the learned discrimination of similar odors (Lei et al., 2013; Lin et al., 2014). In addition, cellular mechanism such as a high threshold for KC activation in *Drosophila* (Turner et al., 2008) and active KC subthreshold properties in locust (Perez-Orive et al., 2002; Jortner et al., 2007) have been shown to support population sparseness. Moreover, plasticity of inhibitory feedback changing response patterns in the KC population

eNeuro Accepted Manuscript

might be crucial for associative learning (Liu and Davis, 2009; Haehnel and Menzel, 2010; Filla and Menzel, 2015; Haenicke et al., 2018). We suggest that different neurophysiological mechanisms of sparseness are not mutually exclusive but rather act in concert. Both lateral inhibition in the AL and feedback inhibition in the MB are likely to be necessary for sparse KC population responses.

Evidently, the sparse connectivity scheme between the PN and KC population is the anatomical basis for population sparse response patterns in the KC layer (e.g. Nowotny et al. 2005; Jortner et al. 2007; Huerta and Nowotny 2009). This connectivity is divergent-convergent with an apparent high degree of randomness (Caron et al., 2013). In our model, connectivity is parametrized by the average number of inputs k per KC and by the synaptic weight w_{PK}. Experimental estimates indicate a small number of inputs per KC. Anatomical data in *Drosophila* provided estimates of $k \approx 13$ (Turner et al., 2008) and $k \approx 5-7$ (Leiss et al., 2009). Szyszka et al. (2005) estimated $k \approx 10$ inputs per KC for the honeybee. For our model we chose $k = 12$. Increasing or decreasing this number resulted in a decrease or increase of population sparseness, respectively (cf. supporting Fig. 4-1). Importantly, with respect to population sparseness, the physiological mechanisms of lateral inhibition and anatomical connectivity parameters represent conceptionally distinct factors. Neuromodulation can affect lateral inhibition on short (tens to hundreds of ms) time scales (Lizbinski and Dacks, 2018). Our results indicate that this modulation could have a drastic effect on population sparseness in the MB. The number of connections, in contrast, can be considered stable on short time scales. However, on a long time scale (days) experience dependent structural plasticity has been demonstrated within the synaptic densities of *Drosophila* MB calyx, where KCs connect to presynpatic PN boutons (Kremer et al., 2010).

Decorrelation of odor representations between AL and MB

Decorrelation of stimulus representations has been postulated to be a fundamental principle underlying sensory processing (Barlow, 1961, 2001). In particular, in the olfactory system odor representations are transformed to decorrelate activity patterns evoked by similar odors making them more distinct (Uchida et al., 2013; Friedrich and Wiechert, 2014; Galizia, 2014). Transformations decreasing the overlap between representations are termed pattern decorrelation. Less overlapping representations increase memory capacity (Treves and Rolls, 1991) and make discrimination of odors easier (Campbell et al., 2013). In our model, we found that AL odor representations preserved the similarity of the input, whereas

eNeuro Accepted Manuscript

representations of similar odors at the periphery became decorrelated in the MB.

We quantified the effects of lateral inhibition and adaptation on pattern correlations. We found that decorrelation of activity patterns in the AL occurred only in the absence of adaptation. Moreover, the amount of decorrelation depended on lateral inhibition strength. Considering decorrelation of odor representations, the difference between lateral inhibition and adaptation is substantial. In our model, lateral inhibition alone sharpens PN responses, whereas adaptation leads to linearization of the input-output relation between the input from ORNs and the PN output (cf. supporting Fig. 2-1). In computational studies lateral inhibition was previously shown to decorrelate odor representations (Luo et al., 2010; Schmuker et al., 2014). In a *Drosophila* study using single sensillum recordings from ORNs and whole-cell recordings from PNs, lateral connection in the AL were found not to affect correlations between glomerular channels (Bhandawat et al., 2007), but there is also evidence for decorrelation of AL representations (Olsen et al., 2010). In our model, pattern correlation between representations of similar odors was preserved at the level of the AL but reduced in the MB. The observed counter-acting effect of adaptation on pattern decorrelation by lateral inhibition in the AL is generally valid for strong adaptation. Strong adaptation currents provide slow, negative feedback that has a linearizing effect on the input-output relation (Ermentrout, 1998). As a consequence of strongly adapting PNs in our model, the pattern correlation of AL odor representations is equal to the pattern correlation given by the tuning profile of the ORN input (cf. Fig. 6).

Odor representation in adaptation currents

Early investigations of dynamical odor representations have shown that odor identity can be reliably decoded from PN spike counts in 50 ms time bins (Stopfer et al., 2003; Mazor and Laurent, 2005; Krofczik et al., 2009). We used this approach to show that odor representations were specific and reliable in our model, including both AL and MB odor representations. We found that odor representation were optimized for discrimination during odor onset (Fig. 7BC). Optimal decoding during stimulus onset is in agreement with electrophysiological evidence from locust and honeybee PNs (Mazor and Laurent, 2005; Krofczik et al., 2009). In the auditory system, Hildebrandt et al. (2015) found that grasshoppers use the onset of a sound pattern as the most reliable information for sound localization. Their study provides behavioral evidence that, in the presence of adaptation, the onset response preserves absolute stimulus levels. Our model shows that at the MB level, stimulus identity

eNeuro Accepted Manuscript

could be decoded from KC spike counts only during a short time window after stimulus onset (up to about 150 ms, cf. Fig. 7B). This is a consequence of the temporally sparse KC responses.

Moreover, we found that KC adaptation currents retain a representation of stimulus identity, resembling a prolonged odor trace (Perisse and Waddell, 2011; Dylla et al., 2013). In our model, an odor trace present in adaptation levels extends well beyond the brief spiking responses. Adaptation currents constitute an internal dynamical state of the olfactory network that is not directly accessible to downstream neurons - a "hidden state" (Buonomano and Maass, 2009). However, adaptation levels influence the responses to (subsequent) stimuli (Farkhooi et al., 2013) and may also affect downstream processing through an indirect pathway.

Our results suggest that odor representations are not exclusively found in the spiking activity. The phenomenological model of spike-triggered adaptation used in this study (see Methods, for review see Benda and Herz, 2003) is motivated by calcium activated outward potassium currents. Those currents are activated by spike triggered calcium influx, which is only slowly removed. We propose that information carried by temporally sparse KC spikes is stored on prolonged time scales by the slowly decaying calcium concentration. We predict long-lasting levels of calcium in the KC population that retain odor information and provide a potential substrate for a short-term sensory memory. Therefore, classification of calcium levels recorded in the MB should reveal odor identity on a time scale determined by the decay of the intracellular calcium level. Indeed, a recent study by Lüdke et al. (2018) showed that prolonged calcium activity in KCs encoded odor information and could be related to behavioral odor recognition performance in trace conditioning experiments where a conditioned odor stimulus is followed by a temporally delayed reinforcement stimulus.

Acknowledgments

This research is supported by the German Research Foundation (grant no. 403329959) within the Research Unit 'Structure, Plasticity and Behavioral Function of the Drosophila mushroom body' (DFG-FOR 2705, https://www.uni-goettingen.de/en/601524.html). RB received a scholarship from the Research Training Group "Sensory Computation in Neural Systems" (DFG-RTG 1589) funded by the German Research Foundation. We thank Farzad Farkhooi for the initial network model and conceptual discussions.

eNeuro Accepted Manuscript

References

Albus, J. S. (1971). A theory of cerebellar function. *Math. Biosci.*, 10(1-2):25–61.

Ardin, P., Peng, F., Mangan, M., Lagogiannis, K., and Webb, B. (2016). Using an Insect Mushroom Body Circuit to Encode Route Memory in Complex Natural Environments. *PLoS Computational Biology*, 12(2).

Assisi, C., Stopfer, M., Laurent, G., and Bazhenov, M. (2007). Adaptive regulation of sparseness by feedforward inhibition. *Nature neuroscience*, 10(9):1176–84.

Barlow, H. (1961). Possible principles underlying the transformations of sensory messages. In *Sensory communication*, volume 6, pages 57–58.

Barlow, H. (2001). Redundancy reduction revisited. *Network: Computation in Neural Systems*, 12(3):241–253.

Belmabrouk, H., Nowotny, T., Rospars, J.-P., and Martinez, D. (2011). Interaction of cellular and network mechanisms for efficient pheromone coding in moths. *Proceedings of the National Academy of Sciences of the United States of America*, 108(49):19790–5.

Benda, J. and Herz, A. V. M. (2003). A universal model for spike-frequency adaptation. *Neural computation*, 15(11):2523–64.

Bhandawat, V., Olsen, S. R., Gouwens, N. W., Schlief, M. L., and Wilson, R. I. (2007). Sensory processing in the Drosophila antennal lobe increases reliability and separability of ensemble odor representations. *Nature neuroscience*, 10(11):1474–82.

Broome, B., Jayaraman, V., and Laurent, G. (2006). Encoding and decoding of overlapping odor sequences. *Neuron*, pages 467–482.

Budick, S. A. (2006). Free-flight responses of Drosophila melanogaster to attractive odors. *Journal of Experimental Biology*.

Buonomano, D. V. and Maass, W. (2009). State-dependent computations: spatiotemporal processing in cortical networks. *Nature Reviews Neuroscience*, 10(2):113–125.

Campbell, R. a. a., Honegger, K. S., Qin, H., Li, W., Demir, E., and Turner, G. C. (2013). Imaging a population code for odor identity in the Drosophila mushroom body. *The Journal of neuroscience : the official journal of the Society for Neuroscience*, 33(25):10568–81.

Capurro, A., Baroni, F., Olsson, S. B., Kuebler, L. S., Karout, S., Hansson, B. S., and Pearce, T. C. (2012). Non-linear blend coding in the moth antennal lobe emerges from random glomerular networks. *Frontiers in neuroengineering*, 5(April):6.

Caron, S. J. C., Ruta, V., Abbott, L. F., and Axel, R. (2013). Random convergence of olfactory inputs in the Drosophila mushroom body. *Nature*, 497(7447):113–7.

Celani, A., Villermaux, E., and Vergassola, M. (2014). Odor landscapes in turbulent environments. *Physical Review X*.

Chou, Y.-H., Spletter, M. L., Yaksi, E., Leong, J. C. S., Wilson, R. I., and Luo, L. (2010). Diversity and wiring variability of olfactory local interneurons in the Drosophila antennal lobe. *Nature neuroscience*, 13(4):439–49.

Deisig, N., Giurfa, M., and Sandoz, J. C. (2010). Antennal lobe processing increases separability of odor mixture representations in the honeybee. *Journal of Neurophysiology*, 103(4):2185–2194.

Demmer, H. and Kloppenburg, P. (2009). Intrinsic membrane properties and inhibitory synaptic input of kenyon cells as mechanisms for sparse coding? *Journal of neurophysiology*, 102(3):1538–50.

eNeuro Accepted Manuscript

Dylla, K. V., Galili, D. S., Szyszka, P., and Lüdke, A. (2013). Trace conditioning in insects-keep the trace! *Frontiers in Physiology*, 4 AUG(August):1–12.

Egea-Weiss, A., Renner, A., Kleineidam, C. J., and Szyszka, P. (2018). High Precision of Spike Timing across Olfactory Receptor Neurons Allows Rapid Odor Coding in Drosophila. *iScience*.

Ermentrout, B. (1998). Linearization of f-i curves by adaptation. *Neural Comput.*, 10:1721.

Faisal, A. A., Selen, L. P. J., and Wolpert, D. M. (2008). Noise in the nervous system. *Nature reviews. Neuroscience*, 9(4):292.

Farkhooi, F., Froese, A., Muller, E., Menzel, R., and Nawrot, M. P. (2013). Cellular Adaptation Facilitates Sparse and Reliable Coding in Sensory Pathways. *PLoS computational biology*, 9(10):e1003251.

Farkhooi, F., Muller, E., and Nawrot, M. (2011). Adaptation reduces variability of the neuronal population code. *Physical Review E*, 83(5):1–4.

Filla, I. and Menzel, R. (2015). Mushroom body extrinsic neurons in the honeybee (Apis mellifera) brain integrate context and cue values upon attentional stimulus selection. *Journal of neurophysiology*, 114:2005–2014.

Fisch, K., Schwalger, T., Lindner, B., Herz, A., and Benda, J. (2012). Channel noise from both slow adaptation currents and fast currents is required to explain spike-response variability in a sensory neuron. *J. Neurosci.*, 32:17332.

Friedrich, R. W. and Wiechert, M. T. (2014). Neuronal circuits and computations: pattern decorrelation in the olfactory bulb. *FEBS letters*.

Froese, A., Szyszka, P., and Menzel, R. (2014). Effect of GABAergic inhibition on odorant concentration coding in mushroom body intrinsic neurons of the honeybee. *Journal of Comparative Physiology A*, 200:183–195.

Fuchs, J. L. and Brown, P. B. (1984). Two-point discriminability: Relation to properties of the somatosensory system. *Somatosensory Research*, 2(2):163–169.

Galili, D. S., Lüdke, A., Galizia, C. G., Szyszka, P., and Tanimoto, H. (2011). Olfactory trace conditioning in Drosophila. *The Journal of neuroscience : the official journal of the Society for Neuroscience*, 31(20):7240–7248.

Galizia, C. G. (2014). Olfactory coding in the insect brain: data and conjectures. *The European journal of neuroscience*, (February):1–12.

Goodman, D. F. M. and Brette, R. (2009). The Brian Simulator. *Frontiers in neuroscience*, 3(2):192–197.

Grünewald, B. (1999). Morphology of feedback neurons in the mushroom body of the honey bee, Apis mellifera. *Journal of Comparative Neurology*, 404(1):114–126.

Gupta, N. and Stopfer, M. (2012). Functional analysis of a higher olfactory center, the lateral horn. *The Journal of neuroscience : the official journal of the Society for Neuroscience*, 32(24):8138–48.

Haehnel, M. and Menzel, R. (2010). Sensory Representation and Learning-Related Plasticity in Mushroom Body Extrinsic Feedback Neurons of the Protocerebral Tract. *Frontiers in Systems Neuroscience*, 4(December):1–13.

Haenicke, J., Yamagata, N., Zwaka, H., Nawrot, M., and Menzel, R. (2018). Neural correlates of odor learning in the presynaptic microglomerular circuitry in the honeybee mushroom body calyx. *eNeuro*, 5(3).

Haider, B., Krause, M. R., Duque, A., Yu, Y., Touryan, J., Mazer, J. A., and McCormick, D. A. (2010). Synaptic and Network Mechanisms of Sparse and Reliable Visual Cortical Activity during Nonclassical Receptive Field Stimulation. *Neuron*.

eNeuro Accepted Manuscript

Hartline, H. K., Wagner, H. G., and Ratliff, F. (1956). Inhibition in the eye of Limulus. *The Journal of general physiology*, 39(5):651–73.

Hildebrandt, K. J., Ronacher, B., Hennig, R. M., and Benda, J. (2015). A Neural Mechanism for Time-Window Separation Resolves Ambiguity of Adaptive Coding. *PLoS Biology*.

Honegger, K. S., Campbell, R. a. a., and Turner, G. C. (2011). Cellular-resolution population imaging reveals robust sparse coding in the Drosophila mushroom body. *The Journal of neuroscience : the official journal of the Society for Neuroscience*, 31(33):11772–85.

Hromádka, T., DeWeese, M. R., and Zador, A. M. (2008). Sparse representation of sounds in the unanesthetized auditory cortex. *PLoS biology*, 6(1):e16.

Huerta, R. and Nowotny, T. (2009). Fast and robust learning by reinforcement signals: explorations in the insect brain. *Neural computation*, 21(8):2123–51.

Isaacson, J. S. (2010). Odor representations in mammalian cortical circuits. *Current opinion in neurobiology*, 20(3):328–331.

Ito, I., Ong, R. C.-Y., Raman, B., and Stopfer, M. (2008). Sparse odor representation and olfactory learning. *Nature neuroscience*, 11(10):1177–84.

Jortner, R. A., Farivar, S. S., and Laurent, G. (2007). A Simple Connectivity Scheme for Sparse Coding in an Olfactory System. *Journal of Neuroscience*, 27(7):1659–1669.

Kanerva, P. (1988). *Sparse Distributed Memory*. MIT Press, Cambridge, MA.

Kee, T., Sanda, P., Gupta, N., Stopfer, M., and Bazhenov, M. (2015). Feed-Forward versus Feedback Inhibition in a Basic Olfactory Circuit. *PLOS Computational Biology*, 11(10):e1004531.

Kloppenburg, P. and Nawrot, M. P. (2014). Neural coding: Sparse but on time. *Current Biology*, 24(19):R957–R959.

Kremer, M. C., Christiansen, F., Leiss, F., Paehler, M., Knapek, S., Andlauer, T. F., Förstner, F., Kloppenburg, P., Sigrist, S. J., and Tavosanis, G. (2010). Structural long-term changes at mushroom body input synapses. *Current Biology*.

Krofczik, S., Menzel, R., and Nawrot, M. P. (2009). Rapid odor processing in the honeybee antennal lobe network. *Frontiers in computational neuroscience*, 2(January):9.

Kuffler, S. W. (1953). Discharge Patterns and Functional Organization of Mammalian Retina. *Journal of Neurophysiology*, 16(1):37–68.

Laughlin, S. B. and Sejnowski, T. J. (2003). Communication in neuronal networks. *Science (New York, N.Y.)*, 301(5641):1870–1874.

Laurent, G. (2002). Olfactory network dynamics and the coding of multidimensional signals. *Nature Rev. Neurosci.*, 3:884.

Lei, Z., Chen, K., Li, H., Liu, H., and Guo, A. (2013). The GABA system regulates the sparse coding of odors in the mushroom bodies of Drosophila. *Biochemical and Biophysical Research Communications*, 436(1):35–40.

Leiss, F., Groh, C., Butcher, N. J., Meinertzhagen, I. A., and Tavosanis, G. (2009). Synaptic organization in the adult Drosophila mushroom body calyx. *J. Comp. Neurol.*, 517(6):808–824.

Lin, A. C., Bygrave, A. M., de Calignon, A., Lee, T., and Miesenböck, G. (2014). Sparse, decorrelated odor coding in the mushroom body enhances learned odor discrimination. *Nature neuroscience*, 17(4):559–68.

eNeuro Accepted Manuscript

766 Liu, X. and Davis, R. L. (2009). The GABAergic anterior paired lateral neuron suppresses and is suppressed by
767 olfactory learning. *Nature neuroscience*, 12(1):53–59.

768 Lizbinski, K. M. and Dacks, A. M. (2018). Intrinsic and Extrinsic Neuromodulation of Olfactory Processing.
769 *Frontiers in Cellular Neuroscience*.

770 Lüdke, A., Raiser, G., Nehrkorn, J., Herz, A. V. M., Galizia, C. G., and Szyszka, P. (2018). Calcium in Kenyon Cell
771 Somata as a Substrate for an Olfactory Sensory Memory in Drosophila. *Frontiers in Cellular Neuroscience*,
772 12:128.

773 Luo, S. X., Axel, R., and Abbott, L. F. (2010). Generating sparse and selective third-order responses in the
774 olfactory system of the fly. *PNAS*, 107(23):10713–8.

775 Marr, B. Y. D. (1969). A theory of cerebellar cortex. *J. Physiol.*, 202(617):437–470.

776 Mazor, O. and Laurent, G. (2005). Transient dynamics versus fixed points in odor representations by locust
777 antennal lobe projection neurons. *Neuron*, 48(4):661–73.

778 Meyer, A., Galizia, C. G., and Nawrot, M. P. (2013). Local interneurons and projection neurons in the antennal
779 lobe from a spiking point of view. *Journal of neurophysiology*, 110(10):2465–74.

780 Mosqueiro, T. S. and Huerta, R. (2014). Computational models to understand decision making and pattern
781 recognition in the insect brain. *Current opinion in insect science*, 6:80–85.

782 Müller, J., Nawrot, M., Menzel, R., and Landgraf, T. (2017). A neural network model for familiarity and context
783 learning during honeybee foraging flights. *Biological Cybernetics*, pages 1–14.

784 Nagel, K. I. and Wilson, R. I. (2011). Biophysical mechanisms underlying olfactory receptor neuron dynamics.
785 *Nature neuroscience*, 14(2):208–16.

786 Nawrot, M. P. (2012). Dynamics of sensory processing in the dual olfactory pathway of the honeybee. *Apidologie*.

787 Nowotny, T., Huerta, R., Abarbanel, H. D., and Rabinovich, M. I. (2005). Self-organization in the olfactory system:
788 One shot odor recognition in insects. *Biological Cybernetics*.

789 Olsen, S. R., Bhandawat, V., and Wilson, R. I. (2010). Divisive normalization in olfactory population codes.
790 *Neuron*, 66(2):287–299.

791 Olsen, S. R. and Wilson, R. I. (2008). Lateral presynaptic inhibition mediates gain control in an olfactory circuit.
792 *Nature*, 452(7190):956–960.

793 Oswald, A.-M. M., Schiff, M. L., and Reyes, A. D. (2006). Synaptic mechanisms underlying auditory processing.
794 *Current opinion in neurobiology*, 16:371–376.

795 Papadopoulou, M., Cassenaer, S., Nowotny, T., and Laurent, G. (2011). Normalization for sparse encoding of odors
796 by a wide-field interneuron. *Science (New York, N.Y.)*, 332(6030):721–5.

797 Pedregosa, F., Varoquaux, G., Gramfort, A., Michel, V., Thirion, B., Grisel, O., Blondel, M., Prettenhofer, P.,
798 Weiss, R., Dubourg, V., Vanderplas, J., Passos, A., Cournapeau, D., Brucher, M., Perrot, M., and Duchesnay,
799 É. (2012). Scikit-learn: Machine Learning in Python. *Journal of Machine Learning Research*, 12:2825–2830.

800 Peng, F. and Chittka, L. (2016). A Simple Computational Model of the Bee Mushroom Body Can Explain Seemingly
801 Complex Forms of Olfactory Learning and Memory. *Current biology : CB*, 0(0):2597–2604.

802 Perez-Orive, J., Mazor, O., Turner, G. C., Cassenaer, S., Wilson, R. I., and Laurent, G. (2002). Oscillations and
803 sparsening of odor representations in the mushroom body. *Science (New York, N.Y.)*, 297(5580):359–65.

804 Perisse, E. and Waddell, S. (2011). Associative memory: Without a trace. *Current Biology*, 21(15):R579–R581.

eNeuro Accepted Manuscript

Rish, I. (2001). An empirical study of the naive Bayes classifier. In *Workshop on empirical methods in artificial intelligence*, volume 22230, pages 41–46.

Schmuker, M., Pfeil, T., and Nawrot, M. P. (2014). A neuromorphic network for generic multivariate data classification. *PNAS*, 111(6):2081–6.

Schwalger, T., Fisch, K., Benda, J., and Lindner, B. (2010). How noisy adaptation of neurons shapes interspike interval histograms and correlations. *PLoS computational biology*, 6(12):e1001026.

Stierle, J. S., Galizia, C. G., and Szyszka, P. (2013). Millisecond stimulus onset-asynchrony enhances information about components in an odor mixture. *The Journal of neuroscience : the official journal of the Society for Neuroscience*, 33(14):6060–9.

Stopfer, M., Jayaraman, V., and Laurent, G. (2003). Intensity versus identity coding in an olfactory system. *Neuron*, 39(6):991–1004.

Strube-Bloss, M. F., Herrera-Valdez, M. a., and Smith, B. H. (2012). Ensemble response in mushroom body output neurons of the honey bee outpaces spatiotemporal odor processing two synapses earlier in the antennal lobe. *PloS one*, 7(11):e50322.

Szyszka, P., Demmler, C., Oemisch, M., Sommer, L., Biergans, S., Birnbach, B., Silbering, A. F., and Galizia, C. G. (2011). Mind the gap: olfactory trace conditioning in honeybees. *The Journal of Neuroscience*, 31(20):7229–39.

Szyszka, P., Ditzen, M., Galkin, A., Galizia, C. G., Menzel, R., Ditzen, M., Galkin, A., and Giovanni, C. (2005). Sparsening and Temporal Sharpening of Olfactory Representations in the Honeybee Mushroom Bodies. *Journal of neurophysiology*, 94(2005):3303–3313.

Szyszka, P., Gerkin, R. C., Galizia, C. G., and Smith, B. H. (2014). High-speed odor transduction and pulse tracking by insect olfactory receptor neurons. *Proceedings of the National Academy of Sciences*.

Szyszka, P., Stierle, J. S., Biergans, S., and Galizia, C. G. (2012). The speed of smell: odor-object segregation within milliseconds. *PloS one*, 7(4):e36096.

Takahashi, N., Katoh, K., Watanabe, H., Nakayama, Y., and Iwasaki, M. (2017). Complete identification of four giant interneurons supplying mushroom body calyces in the cockroach Periplaneta americana. *The Journal of Comparative Neurology*, 525(1):204–230.

Treves, A. (1993). Mean-field analysis of neuronal spike dynamics. *Network: Comput. Neural Syst.*, 4:259.

Treves, A. and Rolls, E. T. (1991). What determines the capacity of autoassociative memories in the brain? *Network: Computation in Neural Systems*, 2(4):371–397.

Turner, G. C., Bazhenov, M., and Laurent, G. (2008). Olfactory Representations by Drosophila Mushroom Body Neurons. *Journal of Neurophysiology*, pages 734 –746.

Uchida, N., Poo, C., and Haddad, R. (2013). Coding and Transformations in the Olfactory System. *Annual review of neuroscience*, (May):363–385.

Van Breugel, F. and Dickinson, M. H. (2014). Plume-tracking behavior of flying drosophila emerges from a set of distinct sensory-motor reflexes. *Current Biology*.

Vickers, N. J. (2000). Mechanisms of animal navigation in odor plumes. *Biological Bulletin*.

Vickers, N. J., Christensen, T. A., Baker, T. C., and Hildebrand, J. G. (2001). Odour-plume dynamics influence file brain's olfactory code. *Nature*.

Vinje, W. E. and Gallant, J. L. (2000). Sparse coding and decorrelation in primary visual cortex during natural vision. *Science (New York, N.Y.)*, 287(5456):1273–1276.

eNeuro Accepted Manuscript

Wessnitzer, J., Young, J. M., Armstrong, J. D., and Webb, B. (2012). A model of non-elemental olfactory learning in Drosophila. *Journal of computational neuroscience*, 32(2):197–212.

Willmore, B. and Tolhurst, D. J. (2001). Characterizing the sparseness of neural codes. *Network*, 12(3):255–270.

Wilson, R. I. (2013). Early olfactory processing in Drosophila: mechanisms and principles. *Annual review of neuroscience*, 36:217–41.

Wilson, R. I. and Laurent, G. (2005). Role of GABAergic inhibition in shaping odor-evoked spatiotemporal patterns in the Drosophila antennal lobe. *The Journal of neuroscience : the official journal of the Society for Neuroscience*, 25(40):9069–79.

Wilson, R. I., Turner, G. C., and Laurent, G. (2004). Transformation of olfactory representations in the Drosophila antennal lobe. *Science (New York, N.Y.)*, 303(5656):366–370.

Wolfe, J., Houweling, A. R., and Brecht, M. (2010). Sparse and powerful cortical spikes. *Current opinion in neurobiology*, 20(3):306–312.

Wüstenberg, D. G., Boytcheva, M., Grünewald, B., Byrne, J. H., Menzel, R., and Baxter, D. a. (2004). Current- and voltage-clamp recordings and computer simulations of Kenyon cells in the honeybee. *Journal of neurophysiology*, 92(4):2589–603.

Yen, S.-C., Baker, J., and Gray, C. (2010). Heterogeneity in the responses of adjacent neurons to natural stimuli in Cat striate cortex. *Journal of Vision*.

eNeuro Accepted Manuscript

Figure Legends

Figure 1 - Olfactory network model structure and odor response. *(A)* Network structure resembles the insect olfactory pathway with three main processing stages. In each glomerulus (dashed circles), a PN (blue) and a LN receive convergent ORN input (red) by one receptor type (RT). Each LN provides unspecific lateral inhibition to all PNs. KCs (orange) receive on average 12 inputs from randomly chosen PNs. *(B)* Receptor response profile (red bars; AL input) depicts the evoked firing rate for each ORN type. Evoked PN spike counts (dashed blue line; AL output) follow the ORN activation pattern. Raster plots depict single trial responses of PNs (blue) and KCs (orange). Presentation of an odor during 1000 ms is indicated by the shaded area. Population firing rates were obtained by averaging over 50 trials. PN spikes display a temporal structure that includes evoked transient responses at stimulus on- and offset, and a pronounced inhibitory post-odor response. PN population rate was averaged over PNs showing "on" responses (blue) and "off" responses (cyan). KC spikes were temporally sparse with majority of the spikes occurring at the stimulus onset. Supporting Fig. 1-1 and Fig. 1-2 (available online) show odor responses with adaptation disabled in the KC and PN population, respectively.

Figure 2 - Lateral inhibition and cellular adaptation shape PN odor response dynamics. *(A)* Single trial PN spiking responses simulated with (right column) and without (left column) lateral inhibition, and with (bottom row) and without (top row) adaptation. Presentation of a single odor during 1000 ms is indicated by the shaded area. With adaptation PNs display a temporal structure that includes a transient and a tonic response, and a pronounced inhibitory post-odor response. *(B)* Trial averaged population firing rate: PNs driven by stimulation (blue) and remaining PNs (cyan). Panels (i)-(iv) indicate presence and absence of lateral inhibition and adaptation as in (A). In the presence of lateral inhibition firing rates during stimulation are reduced. In the presence of lateral inhibition and adaptation (iv) PNs show either transient "on" responses (blue) or "off" responses (cyan). Panels A (iv) and B (iv) are reproduced in Fig. 1B. Supporting Fig. 2-1 (available online) shows PN tuning profiles and input-output relation.

Figure 3 - Odor response dynamics of the KC population. Figure layout as in Fig. 2. *(A)* Single trial population spike raster responses. *(B)* Trial averaged KC population firing rate. Numbers to the right indicate the fraction of activated KCs (n_a) and the mean number of spikes per activated KC during stimulation ($\bar{x}$). Without adaptation (i,ii) KCs spike throughout stimulation because PN drive is strong and persistent. The fraction of activated

eNeuro Accepted Manuscript

KCs drops in the presence of lateral inhibition (ii,iv). With adaptation (iii,iv) most of KC spikes are confined to the stimulus onset, indicating temporally sparse responses. We note that spontaneous KC activity is extremely low (0.03 Hz) in accordance with experimental results (Ito et al., 2008). Panels A (iv) and B (iv) are reproduced in Fig. 1B.

Figure 4 - Quantification of temporal and population sparseness in the KC population. Sparseness was measured in the absence ($\alpha = 0$) and presence ($\alpha = 3$) of lateral inhibition, and the presence (black bars) and absence (gray bars) of spike-frequency adaptation. The sparseness measure was averaged over 50 trials. Error bars indicate standard deviation. A value of one corresponds to maximally sparse responses. *(A)* Adaptation promotes temporal sparseness. *(B)* Lateral inhibition in the AL promotes KC population sparseness. Supporting Fig. 4-1 (available online) shows temporal sparseness when spike-frequency adaptation was disabled in the PN or KC population, and population sparseness for different numbers of PN inputs per KC.

Figure 5 - Lateral inhibition in the AL facilitates population sparseness and reduces pattern correlation in the MB. Spike counts (single trial) of 900 randomly selected KCs in response to two similar odors ("Odor A" and "Odor B") arranged on a 30x30 grid in the absence (top row) and in the presence (bottom row) of lateral inhibition. Inactive KCs are shown in black. *(A)* In the absence of lateral inhibition KCs readily responded to both odors, resulting in an activation pattern where most KCs are active. In the presence of lateral inhibition both odors evoked sparse KC activation patterns. *(B)* Superposition of responses to the two odors. KCs that were activated by both odors are indicated by hot colors (color bar denotes spike count of the stronger response). KCs that were activated exclusively by one of the two odors are indicated in gray. The fraction of KCs that show overlapping responses is reduced in the presence of lateral inhibition. (C) Pattern correlation between the single trial responses in (A) to the two odors obtained for PN (blue) and KC (orange) spikes counts, in the absence ($\alpha = 0$) and presence ($\alpha = 3$) of lateral inhibition. Dashed line indicates pattern correlation of the input (ORNs). Pattern correlation was retained at the AL and reduced at the MB level. Lateral inhibition in the AL reduced pattern correlation in KCs but not in PNs.

Figure 6 - Pattern correlation in the antennal lobe and the mushroom body depend on lateral inhibition strength α. The correlation coefficient ρ_{AB} between the response patterns to two similar odors was calculated and averaged over 50 trials and 5 network realizations for PNs *(blue)* and KCs *(orange)*. Error bars indicate standard deviation

eNeuro Accepted Manuscript

over trials and network realizations. Pattern correlation of the input is indicated by the dashed line. Input correlation is high because similar odors activate largely overlapping set of receptors. *(A)* In the presence of adaptation, pattern correlation in PNs (*blue*) stays close to the input correlation for all values of lateral inhibition strength. In KCs (*orange*) the correlation decreases for small values of lateral inhibition strength, and increases for large values of lateral inhibition strength. Pattern correlation in KCs is minimal for $\alpha = 3$. *(B)* In the absence of adaptation, pattern correlation decreases with the lateral inhibition strength both in PNs and KCs. The decrease is stronger in KCs. *(CD)* Pattern correlation $\tilde{\varrho}_{AB}$ was calculated based on evoked, trial-averaged spike counts in the presence (C) and absence (D) of lateral inhibition. The correlation coefficient between the trial-averaged response patterns to two similar odors was calculated and averaged over 5 network realizations. Error bars indicate standard deviation over network realizations. In the presence of adaptation (C) the overlap between trial-averaged KC representations of two similar odors (orange) shows a minimum for intermediate strengths of lateral inhibition ($1 \leq \alpha \leq 3$). At the minimum, the KC overlap is below the overlap between trial-averaged PN representations. In the absence of adaptation the overlap between trial-averaged KC representations is generally lower than the overlap between trial-averaged PN representations for all strengths of lateral inhibition. Supporting Fig. 6-1 and Fig. 6-2 (available online) show the mean fraction of activated KCs and mean pairwise KC cross-correlation, respectively.

Figure 7 - Decoding of odor identity indicates a prolonged and reliable odor information in KC adaptation currents. *(A,B,D)* Decoding accuracy was calculated for non-overlapping 50 ms time bins, based on a set of seven stimuli (chance level ≈ 0.14) presented for one second (shaded area). Blue shading indicates standard deviation obtained from a cross-validation procedure (see Methods). *(A)* Decoding of odor identity from PN spike counts. Decoding accuracy peaks at odor on- and offset, and remains high after stimulation. *(B)* Decoding of odor identity from KC spike counts. Decoding accuracy is above chance only in the first three bins following stimulus onset. *(C)* Adaptation current amplitudes (single trial, hot colors in arbitrary units) of 100 selected KCs in response to "odor A" (top) and "odor B" (bottom). *(D)* Decoding of odor identity from KC adaptation currents. Decoding accuracy peaks 150 ms after odor onset, then drops during stimulation but remains high and is sustained after odor offset.

Supporting Figure 1-1: Odor response with selective adaptation in the LN and the PN population. Strong phasic PN input elicits phasic KC responses. High KC firing threshold

eNeuro Accepted Manuscript

ensures sparse responses in the absence of SFA in the KC population.

Supporting Figure 1-2: Odor response with selective adaptation in the LN and the KC population. The absence of SFA in the PN population was compensated by a constant current $I_0 = 0.38$ nA. PNs show a constant population rate response with a slightly delayed onset due to inhibition by LNs. KCs show a strong onset population rate response and a non-zero tonic firing rate.

Supporting Figure 2-1: In the absence of adaptation (A,B), lateral inhibition (B) sharpens the PN tuning profile (blue). In the presence of adaptation (C,D) the PN tuning profile is not affected by lateral inhibition. The tuning profile was obtained by averaging PN firing rates during the one second stimulation window and across 50 trials. PNs receive input from ORNs of the corresponding type according to the receptor response profile. The receptor response profile (gray), rescaled between the minimum and maximum PN firing rate, is shown in all panels for comparison. The insets show the input-output relation between the ORN and the PN firing rates. Both, averaged (blue line) and single trial (gray crosses) PN firing rates are shown.

Supporting Figure 4-1: (A) Temporal sparseness with SFA presence in selected populations. *Black:* PNs, LNs and KCs. *White dashed:* LNs and KCs. *White:* LNs and PNs. *Gray* bars indicate simulation in the complete absence of SFA. **(B)** Population sparseness depends on the mean number of PN inputs per KC k, both in the absence ($\alpha = 0$, left) and presence ($\alpha = 3$) of lateral inhibition. In comparison with the default number of PN inputs ($k = 12$, black bars), reducing the mean number of connections to $k = 9$ (white dashed bars) increased population sparseness, whereas increasing the mean number of connections to $k = 15$ (white bars) decreased population sparseness. The gray bar corresponds to $k = 12$ in the absence of SFA and is given for reference.

Supporting Figure 6-1: Mean fraction of activated KCs for different strengths of lateral inhibition. We obtained the fraction of activated KCs by counting KCs that have fired at least one spike during one of the given epochs: one second of stimulation, one second of spontaneous activity, and first 50 ms after stimulus onset (transient response). **(A)** In the presence of spike-frequency adaption the mean fraction of activated KCs during evoked activity (blue) shows a minimum for intermediate strength of lateral inhibition. At the minimum, around 10% of the KCs responded to the stimulus. This fits well to the experimentally reported values in the range of 5-11% (Turner et al., 2008; Honegger et al., 2011). **(B)** In the absence of spike-frequency adaption the mean fraction of activated

KCs decreases with lateral inhibition during evoked activity (blue). Note that for $\alpha > 4$ the fraction of responding KCs is close to zero, or zero. In the absence of spike-frequency adaption, and higher strengths of inhibition, KCs do not receive strong enough inputs to spike.

Supporting Figure 6-2: Mean pairwise PN cross-correlation for different strengths of lateral inhibition. For each PN, a vector obtained by binning the corresponding spike train into 50 ms windows was calculated. Pairwise correlation between the vectors was calculated and averaged over all PN pairs and 50 trials.

eNeuro Accepted Manuscript

eNeuro Accepted Manuscript

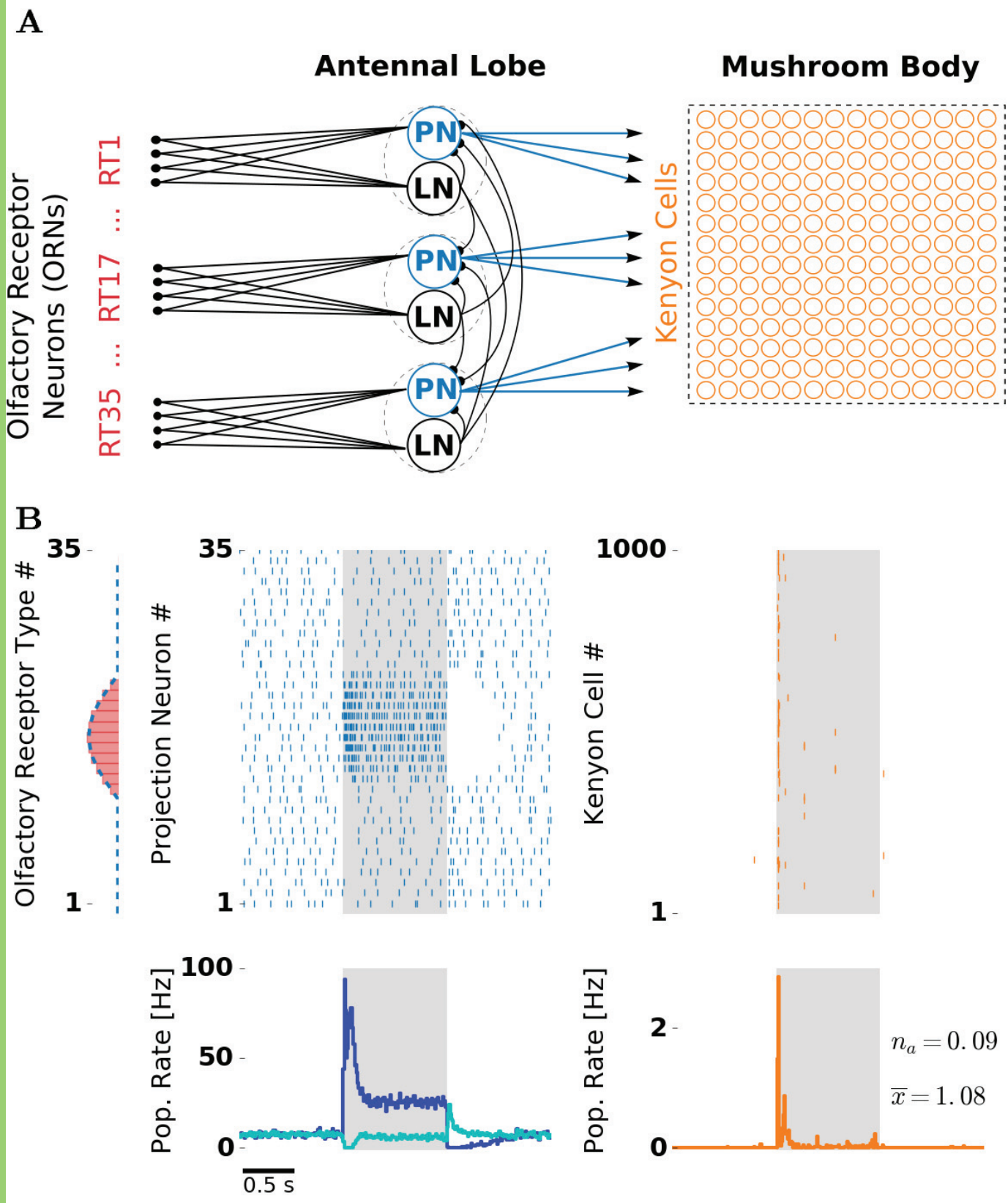

eNeuro Accepted Manuscript

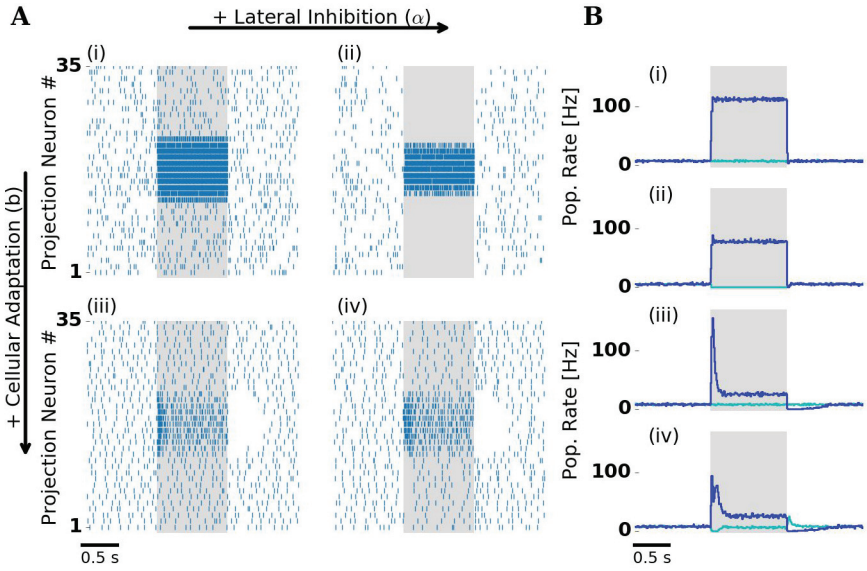

eNeuro Accepted Manuscript

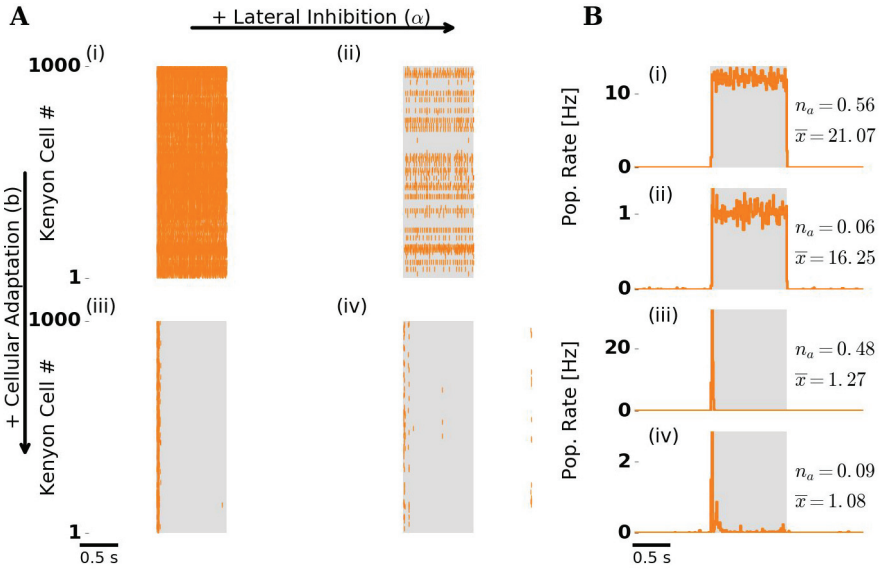

eNeuro Accepted Manuscript

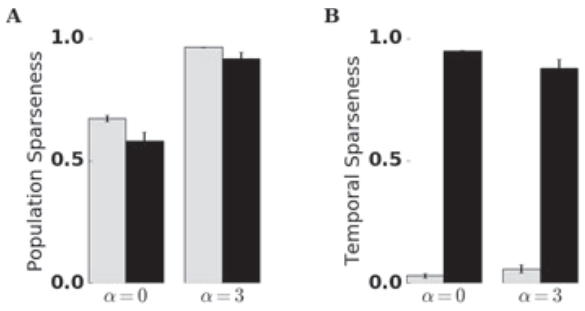

eNeuro Accepted Manuscript

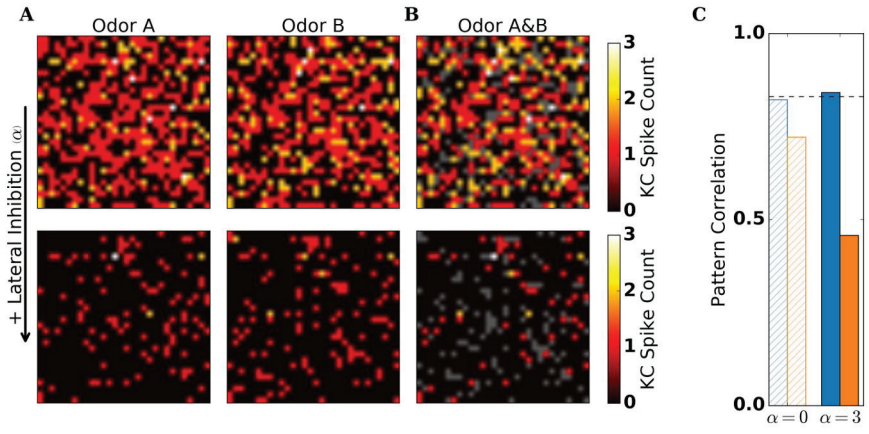

eNeuro Accepted Manuscript

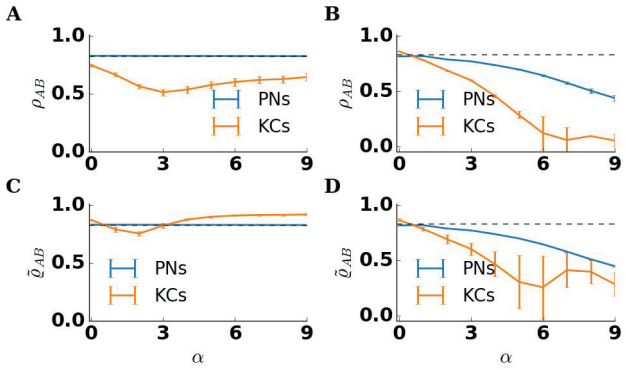

eNeuro Accepted Manuscript